Proceedings of the 2nd World Congress on Mechanical, Chemical, and Material Engineering (MCM'16)
Budapest, Hungary – August 22 – 23, 2016
Paper No. HTFF 130
DOI: 10.11159/htff16.130

Heat Transfer Correlations for Refrigerated Containers

Nuri Kayansayan[1], Ersin Alptekin[2], Mehmet Akif Ezan[2]
[1]Department of Mechanical Engineering, Near East University
Mersin, 10,Turkey
nuri.kayansayan@deu.edu.tr
[2]Department of Mechanical Engineering, Dokuz Eylül University
İzmir, 35397, Turkey
ersin.alptekin@deu.edu.tr; mehmet.ezan@deu.edu.tr

Abstract - A numerical study of conjugated heat transfer in ceiling-slot refrigerated containers is carried out to analyze the temperature distribution effectiveness. The refrigerated container is represented by a fixed cross-sectional area but its length sequentially varied as 6.13m, 8.33m, and 13.3m, and is under turbulent flow regime. Besides, the effect of slot size on thermal characteristics is studied by considering half-span injection. The container walls are defined as conductive opaque and are interacting with outside environment. The air velocity at the slot exit is varied depending upon the injection Reynolds number between $2x10^4 \leq Re \leq 2x10^5$. The gravity effect is taken into account, and the coupled mass, momentum, and energy equations are discretized in finite volumes by implementing the Reynolds Stress Model to predict the turbulence stresses. The resulting heat transfer coefficients are presented as plots of the mean Nusselt number versus the modified Reynolds number.

Keywords**:** Flow analysis, heat transfer analysis, computational fluid dynamics, refrigerated container

Nomenclature

A	Cross-sectional area, m^2
C's	Turbulence model coefficients, dimensionless
c_p	Specific heat of air, $Jkg^{-1}K^{-1}$
d_h	Hydraulic diameter of the injection slot, m
E	Temperature effectiveness, dimensionless
Gr	Grashof number, $g\beta\Delta TH^3/\nu^2$, dimensionless
H	Container height, m
h	Convective heat transfer coefficient, $Wm^{-2}K^{-1}$
I_{solar}	Solar irradiation reaching the earth surface, Wm^{-2}
k	Kinetic energy of turbulence, m^2s^{-2}
L	Container length, m
l	Related to evaporator size, see Fig. 1, m
Nu	Nusselt number, hH/λ, dimensionless
Pr	Prandtl number, $\mu c_p/\lambda$, dimensionless
p	Pressure, Pa
q	Heat transfer rate through a conductive surface, W

Greek letters

α_s	Surface absorptivity, dimensionless
ε	Turbulence energy dissipation rate, m^2s^{-3}
ε_s	Surface emissivity, dimensionless
λ	Thermal conductivity, $Wm^{-1}K^{-1}$
μ	Dynamic viscosity, $kgm^{-1}s^{-1}$
ϑ	Volume flow rate, m^3s^{-1}
ρ	Air density, kgm^{-3}

Subscripts

cr	critical
in	Inlet to evaporator
inj	Exit from evaporator
i,j,k	Vector directions in x,y,z
J	Identifies a conductive surface
m	Mean value
s	Surface inside
so	Surface outside
t	Turbulent
w	Wall

1. Introduction

There exists scarce research work on refrigerated containers with conjugated heat transfer involving conduction and mixed convection in turbulent flow regime [1, 2, 3]. The aim of this research work is to carry out a numerical analysis on conjugated heat transfer inside a refrigerated container with heat conductive walls, and to analyze the effect of the container shape factor (L/H), and the Reynolds number of supplied cold air (Re) on the temperature distribution

effectiveness. As shown in Fig. 1, the frigorific container is modeled as rectangular cavity and the conductive walls are set as opaque. For this study, the height $(H = 2.5\ \text{m})$ and the width $(W = 2.46\ \text{m})$ dimensions of the container are kept constant but the container length assumes values of $L = 6.13\ \text{m},\ 8.33\ \text{m},\ 13.3\ \text{m}$ sequentially. The construction material for the conductive walls is composed of a layer of polyurethane foam (70mm) sandwiched between two layers of very thin (0.5mm) sheet metal of steel.

2. Problem Definition and Modelling

The physical model under analysis is a three dimensional cavity and air inside of the container is initially assumed to be at uniform temperature. In Fig. 1, the front panel of the container sustains the refrigeration equipment and hence reinforced by additional supporting layers with low thermal conductivity and the bottom panel is heavily constructed.

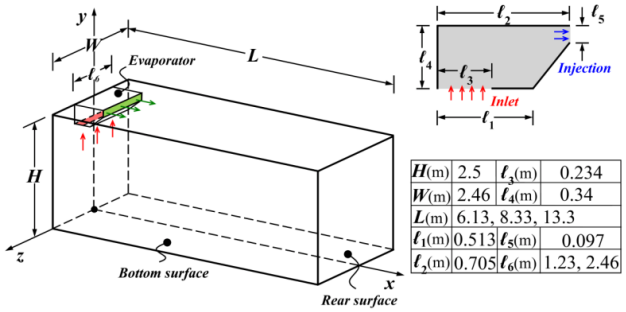

H(m)	2.5	ℓ_3(m)	0.234
W(m)	2.46	ℓ_4(m)	0.34
L(m)	6.13, 8.33, 13.3		
ℓ_1(m)	0.513	ℓ_5(m)	0.097
ℓ_2(m)	0.705	ℓ_6(m)	1.23, 2.46

Fig. 1: Container geometry and the dimensions of the evaporator used in the analysis.

Hence both surfaces are assumed to be adiabatic. However, heat is conducted through the rest of the container walls producing a temperature gradient between that particular wall surface and the air inside the container.

2.1. Convective model for air inside the container

In determining flow and heat transfer characteristics of internal airflow of the refrigerated container time averaged mass, momentum, and energy equations are:

$$\frac{\partial}{\partial x_i}\left(\rho u_i\right) = 0 \tag{1}$$

$$\frac{\partial}{\partial x_j}\left(\rho u_i u_j\right) = -\frac{\partial p}{\partial x_i} + \frac{\partial}{\partial x_j}\left[\mu\left(\frac{\partial u_i}{\partial x_j} + \frac{\partial u_j}{\partial x_i}\right) - \rho\overline{u_i' u_j'}\right] - \rho g_i \beta_i \left(T - T_\infty\right) \tag{2}$$

$$\frac{\partial}{\partial x_i}\left(\rho u_i T\right) = \frac{1}{c_p}\frac{\partial}{\partial x_j}\left[\lambda\frac{\partial T}{\partial x_j} - \rho c_p \overline{u_j' T'}\right] \tag{3}$$

where the turbulence stresses have to be predicted by Reynolds Stress Model (RSM). There are many versions of RSM, and the one used in the present study is for time averaged turbulent viscosity and includes sudden changes in the strain rate, and secondary flows. Due to symmetry of the flow, gradients of all transport properties have to be zero at the symmetry surface, and no slip condition at the container walls is satisfied by $(u = v = w)_{wall} = 0$. Reynolds number and the hydraulic diameter are defined respectively as,

$$\text{Re} = \frac{\rho u_{inj} d_h}{\mu} \qquad \text{and} \qquad d_h = \frac{2 l_5 l_6}{\left(l_5 + l_6\right)} \tag{4}$$

To analyze the distinct operational modes in applications and study the effect of flow rate on thermal characteristics, air velocity at the injection slot is varied in a range between 1.38m/s and 13.88m/s. Hence, at these moderate velocities, the turbulence intensity at the slot exit is taken to be 10-percent. The condition of no change in transport properties at the

suction slot is satisfied by $\partial\varepsilon/\partial n=0$ and $\partial k/\partial n=0$ [4]. Since the front and bottom surfaces are adiabatic then $\partial T/\partial n=0$ and at the suction slot, $\partial T/\partial n=0$ for returned air.

2.2. Conductive model

Three dimensional governing equation for heat conduction through a particular conductive wall i.e., top, lateral, or rear wall, is as follows,

$$\frac{\partial}{\partial x}\left(\lambda_w\frac{\partial T_w}{\partial x}\right)+\frac{\partial}{\partial y}\left(\lambda_w\frac{\partial T_w}{\partial y}\right)+\frac{\partial}{\partial z}\left(\lambda_w\frac{\partial T_w}{\partial z}\right)=0 \tag{5}$$

where, λ_w and T_w are respectively the thermal conductivity, and the temperature of a particular conductive wall. The boundary condition at the inside surface of the conductive walls is,

$$q_{cond-w}=q_{gain} \tag{6}$$

However, on the outside surface, due to effect of solar radiation and forced convection, the container gains heat in accord with the following relation,

$$\left(q_{gain}\right)_J=\alpha_s\left(I_{solar}\right)_J-\sigma\varepsilon_s\left(T_{soJ}^4-T_{sky}^4\right)-h_{\infty J}\left(T_{soJ}-T_\infty\right) \tag{7}$$

where *J* indicates a particular conductive wall. All external surfaces of conductive walls are assumed to be white painted metallic substrate with $\alpha_s=0.21$, and $\varepsilon_s=0.96$ [5] and exposed to a large environment with a view factor of unity. In Eq. (7), the monthly averaged values of solar irradiation intensity, $\left(I_{solar}\right)_J$ is provided by the Joint Research Center of European Commission [13].

2.3. Convective model for external flow around the container

Determination of heat transfer coefficients of the outer surfaces, $h_{\infty J}$, in Eq. (7) first requires the flow field around the refrigerated truck to be analyzed by RANS equations as follows,

$$\frac{\partial}{\partial x_j}\left(\rho u_i u_j\right)=-\frac{\partial p}{\partial x_i}+\frac{\partial}{\partial x_j}\left[\mu\left(\frac{\partial u_i}{\partial x_j}+\frac{\partial u_j}{\partial x_i}\right)-\rho\overline{u_i'u_j'}\right] \tag{8}$$

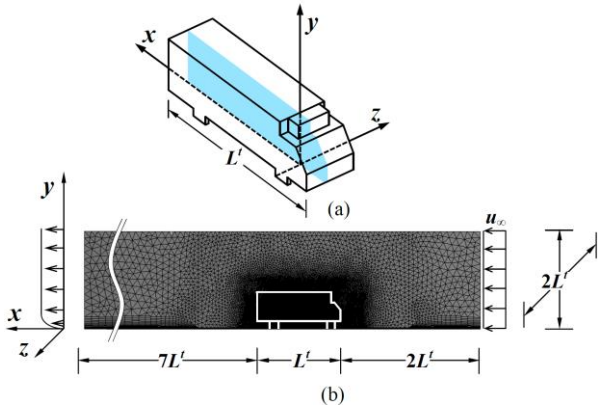

Fig. 2: (a) 3-D view of experimental truck, (b) Computational domain for flow around the truck.

the turbulent energy equation (Eq. 3) is implemented to get the temperature field and the temperature gradients on the outer surfaces of top, lateral and rear walls. As shown in Fig. 2, Atmospheric air at 298K enters the solution domain uniformly at a speed of 25m/s with turbulent intensity of 2-percent, and the turbulent viscosity ratio (μ_t / μ) at 10.At the exit of computational domain, however, flow is fully developed and no change in transport properties takes place. Similarly, at the symmetry surface, gradients of all transport properties are taken to be zero. The thermal boundary condition at the outer surface of a conductive wall requires that

$$-\lambda\left(\frac{\partial T}{\partial n_J}\right)_{n_J=0} = h_{\infty J}\left(T_{soJ} - T_\infty\right) \tag{9}$$

where the temperature gradient at a particular surface, *J*, is predicted by solving the temperature field of the external flow as described above. Computations for external flow analysis are carried out by the application of realizable $k-\varepsilon$ turbulence modelling [6].

3. Numerical Solution Method

For the entire computational domain inside the container, quadrilateral meshes are used. For the external flow around the truck, however, computations in the vicinity of walls are provided by quadrilateral meshes but the rest of domain is filled with tetrahedral type of meshes. The pressure correction algorithm SIMPLE is used for solving momentum equations and the coupled energy equation. Convective terms are discretized by the upwind scheme and diffuse terms by the centered scheme. Computations start with the application of k-ε turbulence modelling. After attaining convergence for all variables, Reynolds Stress Model (RSM) of turbulence is applied for predicting the Reynolds stresses and then the discretization scheme is changed from upwind to QUICK method. To avoid occurrence of instabilities in the solution due to gravity effects, a stepwise solution procedure is employed for flow inside the container. At each step of solution, the magnitude of the gravity term in the momentum equation is gradually increased until $g = 9.81\ \text{m/s}^2$ is attained. Then the total heat gained by the internal surfaces of conductive walls is computed and compared with the counterpart value evaluated at the outer surfaces. A deviation error of 0.1-percent or less is assumed to be acceptable for a solution inside of the container. Otherwise, new values to temperatures at the outer surfaces of conductive walls are assigned by Eq. (7), and then the entire computations are repeated until the thermal conditions are satisfied. A mesh independency analysis is carried out for the largest container of length; $L = 13.3$ meters. The results of velocity and temperature distributions inside the container are obtained for conditions of $\text{Re} = 10^5$, and $T_{inj} = 263\text{K}$ at the outlet of injection slot. Four cases of mesh size density variations are considered in mesh independency analysis. Respect to the node arrangement in length x height x width, the number of nodes for each case is given as; Case A: $509\times136\times89$, Case B: $442\times119\times78$, Case C: $348\times94\times62$, and Case D: $311\times85\times58$. The following parameters are compared for the mesh independency: 1. Velocity along the slot jet symmetry line, 2. Flow separation point from the injection slot exit, 3. Velocity distributions at several x-locations for both vertical (x-y plane) and horizontal (x-z plane) symmetry surfaces of the injection slot, and 4. Temperature profiles at locations of $x = 2\text{m}, 8.2\text{m}, \text{and } 10.5\text{m}$ in lengthwise direction of the container. In actual values of velocity and temperature, expressing the computational error as, $\left|\hat{y}_B - \hat{y}_A\right| \times 100 / \hat{y}_A$, the maximum error being 4.7% in velocity and 0.005% in temperature at the symmetry surface for $x = 10.5\text{m}$ corresponds respectively to 0.32 m/s and 0.013 K of deviations. Hence the mesh size with $442\times119\times78$ nodes (Case *B*) is decided to be satisfactory for present analysis. In discretization of the conductive walls, 6 control volumes in the direction of wall thickness are considered for all configurations. A large number of nodes have to be used in describing the external flow, and the number increases as the container length increases. Hence, the number of nodes used in the external flow for container lengths of $L = 6.13\text{m}$, 8.33m and 13.3m respectively is as follows: 29.486x10^6, 35.065x10^6 and 47.689x10^6.

4. Result and Discussion

In analyzing four values of air injection velocity are chosen: 1.38m/s, 3.47m/s, 6.94m/s, and 13.88m/s and their corresponding Reynolds numbers in sequence are 2×10^4 , 5×10^4 , 1×10^5 and 2×10^5 .Richardson number of the flow

varies in a range between 0.2 and 0.5 for all aspect ratios and for the minimum flow rate studied at $\mathrm{Re} = 2\times10^4$. The variation range of Richardson number signifies the occurrence of mixed convection currents in the container at low flow rates [7] and the gravity effect is taken into account. Fig. 3 presents the streamlines at the symmetry surface for various values of Reynolds number and for the container configuration of $L/H = 5.32$. As the flow rate increases, the decrease in the size of secondary circulation zone is distinctly illustrated by this figure. Likewise, it can be observed by Fig. 4 that the distribution of isothermals at the symmetry surface substantiates the flow behavior in the secondary circulation zone of the container. The isotherm at $T = T_{in}$ divides the container into two perfectly defined regions identified as hot and cold zones.

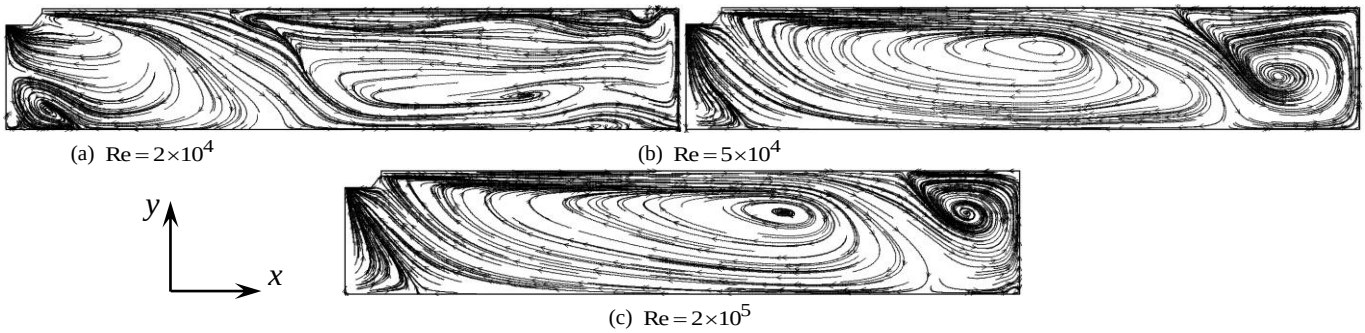

(a) $\mathrm{Re} = 2\times10^4$ (b) $\mathrm{Re} = 5\times10^4$

(c) $\mathrm{Re} = 2\times10^5$

Fig. 3: Flow behavior at L/H = 5.32 for various Reynolds numbers.

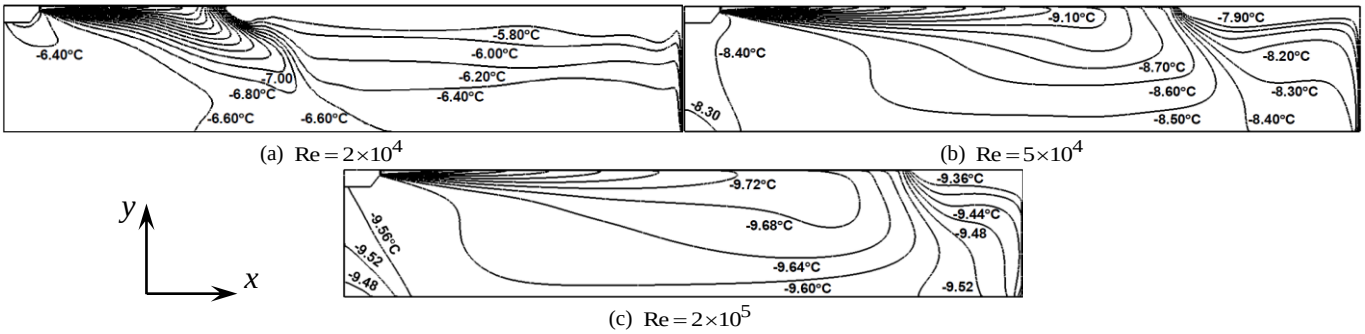

(a) $\mathrm{Re} = 2\times10^4$ (b) $\mathrm{Re} = 5\times10^4$

(c) $\mathrm{Re} = 2\times10^5$

Fig. 4: Isotherms for the container with L/H = 5.32 at various Reynolds numbers.

In Fig. 4a, air is thermally stratified for temperatures, $T > -6.14°\mathrm{C}$, and becomes stagnant in a region close to the hot top surface of the container. As the flow rate increases as in Figs. 4b and 4c, the extend of the hot zone clearly decreases. Fig. 5 demonstrates isotherms for $L/H = 2.45$, 3.33, and for various Reynolds number. For configuration at $L/H = 2.45$, the warmest zone takes place in the central part over which the main flow circulates, and for $L/H = 3.33$, due to existence of secondary circulation region by flow separation at $\mathrm{Re} = 2\times10^4$, the critical zone occurs at the upper region close to the intersection of top and rear walls.

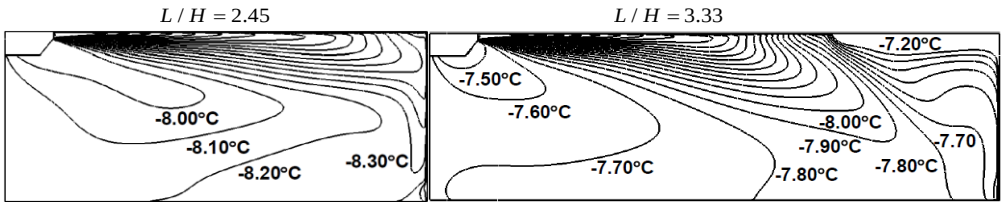

(a) $\mathrm{Re} = 2\times10^4$

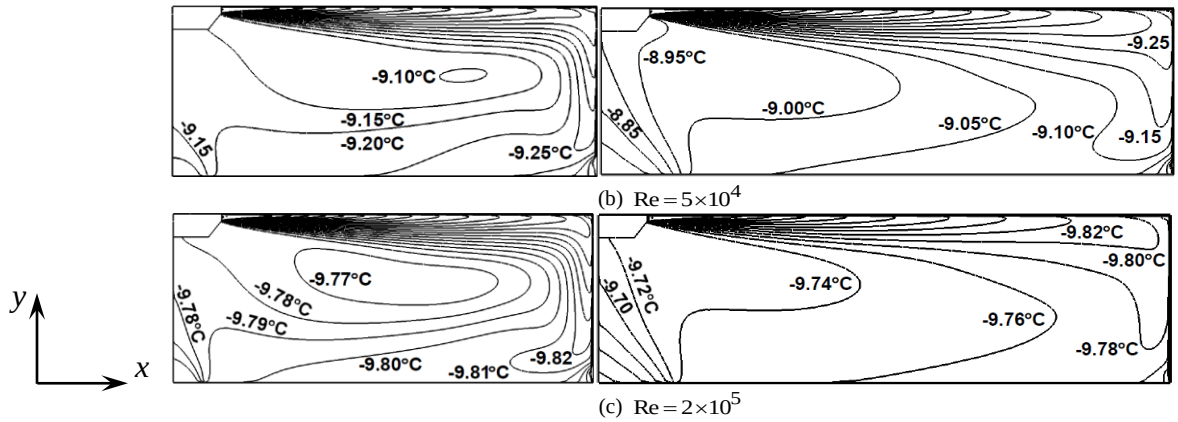

Fig. 5: Isotherms for two different container configurations and at various Reynolds numbers.

Temperature distribution effectiveness indicates the way in which temperature patterns is distributed along the container and is defined as following,

$$E = \frac{T_{in} - T_x}{T_{in} - T_{inj}} \tag{10}$$

where, T_x, is the mass flow weighted average temperature of air at a location, x, and is determined by,

$$T_x = \frac{\int_A \rho c_p T |u| dA}{\int_A \rho c_p |u| dA} \tag{11}$$

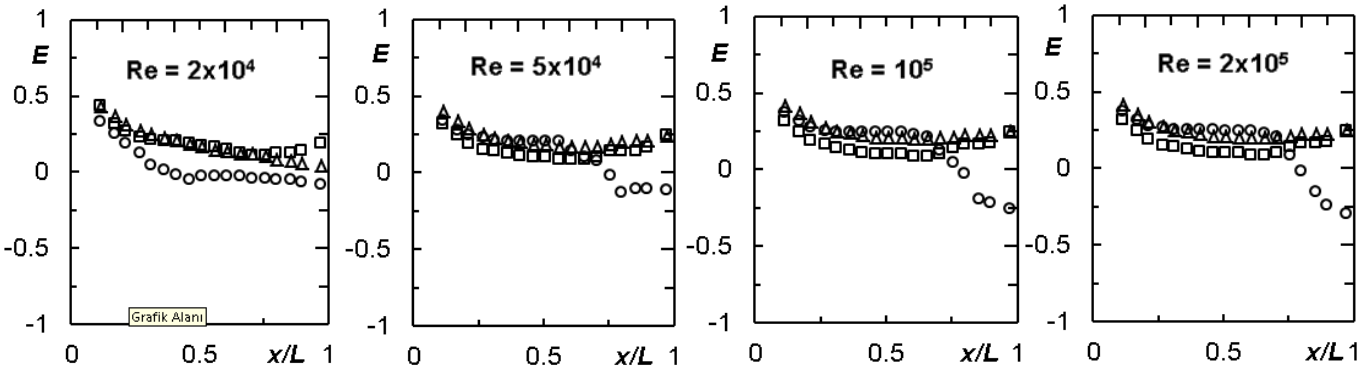

(a) (b)(c)(d)

Fig. 6: Temperature distribution effectiveness for container configurations of L/H = 5.32 (○), 3.33 (△), 2.45 (□) and at various Reynolds numbers.

The T_x values are calculated for 40 (y-z) planes separated with an increment of $x/L = 0.0245$ from each other and E distributions for half-span injection containers with conductive walls having 0.07m thick of insulation layer are shown in Fig.6.The average Nusselt number of a particular conductive surface is a parameter to quantify heat transfer rate inside the container and is defined as the ratio of convection heat transfer over the conduction heat flux at that particular Jth-surface as following,

$$Nu_J = \frac{-\lambda}{q_{ref}} \int_A \left| \left(\frac{\partial T}{\partial n} \right)_{n=0} \right|_J dA_J \tag{12}$$

where n indicates the normal direction at a particular conductive wall of J and q_{ref} is the reference conduction heat transfer given by $q_{ref} = \lambda A(T_{sJ} - T_m)/H$ with T_{sJ} is the average inside surface temperature of surface J and T_m is the mean air temperature inside the container.

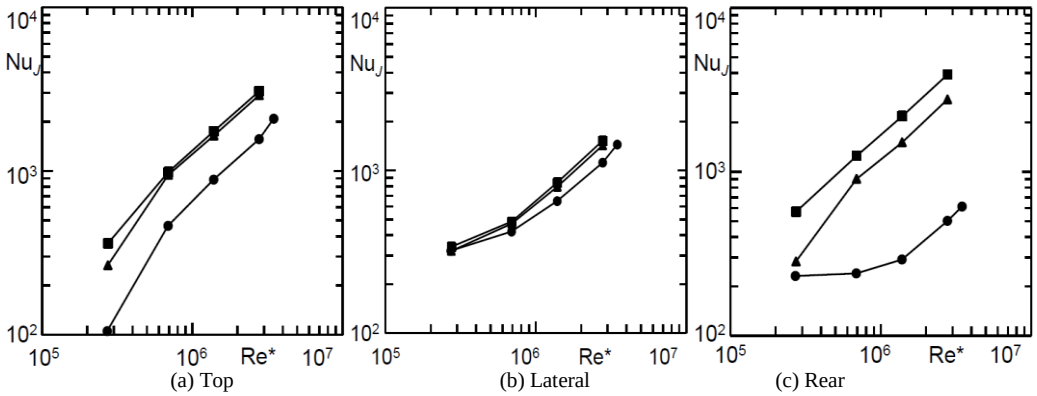

(a) Top (b) Lateral (c) Rear

Fig. 7: Average Nusselt number of inside surfaces of conductive walls at L/H = 5.32 (●), 3.33 (▲), and 2.45 (■).

To specify the average heat transfer over the inside surfaces of conductive walls of the container, the average Nusselt number (Nu_J) has to be determined. In accord with Eq. (12), the Nusselt number at a particular surface is generated by numerically integrating the temperature gradients on that surface, and the results are illustrated in Fig. 7. Especially in mixed convection mode, the container height, H, plays an important role in flow characterization and the modified Reynolds number, $\mathrm{Re}^* = V_{inj} H/\nu$, is implemented to describe the results in Fig. 7. For all container configurations and at their respective surfaces, Nusselt number tends to increase as the Reynolds number increases. However, in Fig. 7c, due to slow motion of convection currents at the rear surface of the container with $L/H = 5.32$, the Nusselt number exhibits rather small tendency to increase in the range of modified Reynolds numbers between 3×10^5 and 10^6. In general, it can be assessed that the heat transfer is higher for configurations $L/H = 2.45$ and 3.33 regarding to configuration of $L/H = 5.32$ at all surfaces. In determining the mean Nusselt number of a ceiling-slot ventilated container, the area based mean temperature, T_{sm} of conductive surfaces is first calculated for a total of 13 numerical runs at 3 different container geometries, and then considering the total heat gain, $\sum_J q_J$, for a specified flow and geometric conditions, the overall averaged heat transfer coefficient and consequently the mean Nusselt number (Nu_m) may be computed as,

$$h_m = \sum_J q_J \Big/ (T_{sm} - T_m) \sum_J A_J \quad \text{and} \quad \mathrm{Nu}_m = h_m H/\lambda \tag{13}$$

Referring to the results as shown in Fig. 8, the least square linear regression analysis applied to the studied cases of half-span injection yields the following correlation,

$$\mathrm{Nu}_m = 0.041(\mathrm{Re}^*)^{0.76} \left(L/H\right)^{-0.63} \tag{14}$$

in which, $2.7\times10^5 \le \mathrm{Re}^* \le 3.5\times10^6$, and $2.45 \le L/H \le 5.32$. This equation represents the numerical data with a maximum deviation of 10.8%, and provides a correlation coefficient of R=0.994. The thermo-physical properties in eq. (14) are evaluated at the container mean temperature, T_m.

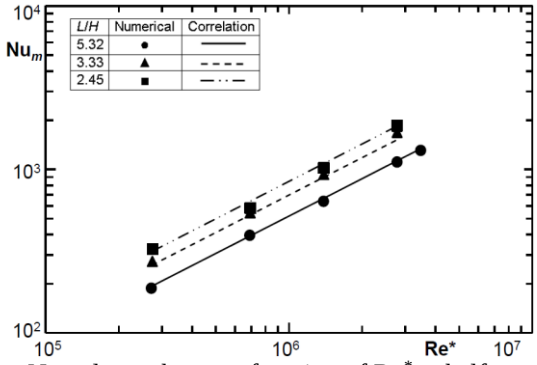

Fig. 8: Mean Nusselt number as a function of Re^* at half-span injection.

5. Conclusion

In this paper a numerical study of conjugated heat transfer inside a ceiling-slot ventilated container on turbulent flow regime is presented; where convective heat transfer inside the container is coupled to heat conduction through opaque walls is analyzed. Three different aspect ratios at half-span size of the slot is considered for numerical study. The Reynolds number of injection varies in the range between 2×10^4 and 2×10^5 so that air velocities needed for refrigerated truck applications are adequately covered. Based on the results it can be concluded that

1. Referring to temperature distribution effectiveness, the container with an aspect ratio of 3.33 shows the highest effectiveness for the range of Reynolds numbers (Re) studied.

2. A Correlation for the mean Nusselt number respect to modified Reynolds number is presented for the ceiling-slot ventilated containers having half-span injection. The correlation is valid for modified Reynolds numbers in the range of 2.7×10^5 and 3.5×10^6 and for the container aspect ratios varying between 2.45 and 5.32.

References

[1] J. Moureh and D. Flick, "Airflow characteristics within a slot-ventilated enclosure," *Int. J. Heat and Fluid Flow*, vol. 26, pp. 12-24, 2005.

[2] N. J. Smale, J. Moureh and G. Cortella, "A review of numerical models of airflow in refrigerated food applications," *Int. J. Refrigeration*, vol. 29, pp. 911-930, 2006.

[3] Q. Chen, "Comparison of different *k-ε* models for indoor air flow computations," *Numerical Heat Transfer, Part B*, vol. 28, pp. 353-369, 1995.

[4] S. Cao and J. Meyers, "Influence of turbulent boundary conditions on RANS simulations of pollutant dispersion in mechanically ventilated enclosures with transitional slot Reynolds number," *Building and Environment*, vol. 59, pp. 397-407, 2013.

[5] T. L. Bergman, A. S. Lavine, F. P. Incropera and D. P. DeWitt, Fundamentals of Heat and Mass Transfer, 7th edition, John Wiley and Sons, 2011.

[6] T. H. Shih, W. W. Liou, A. Shabbir, Z. Yang and J. Zhu, "A New *k-ε* Eddy-Viscosity model for high Reynolds number turbulent flows," *Computers and Fluids*, vol. 24, pp. 227-238, 1995.

[7] T. S. Cheng, "Characteristics of mixed convection heat transfer in a lid-driven square cavity with various Richardson and Prandtl numbers," *Int. J. Thermal Sciences*, vol. 50, pp. 197-205, 2011.